PNAS
www.pnas.org

Supplementary Information for

Self-cleavage of the *glmS* Ribozyme Core is Controlled by a Fragile Folding Element

Andrew Savinov[1] and Steven M. Block[2,3]

[1]Biophysics Program, Stanford University, Stanford, CA 94305, USA.
[2]Department of Applied Physics, Stanford University, Stanford, CA 94305, USA.
[3]Department of Biology, Stanford University, Stanford, CA 94305, USA.

Corresponding author: Steven M. Block

Email: sblock@stanford.edu

This PDF file includes:

www.pnas.org/cgi/doi/10.1073/pnas.1812122115

Supplementary Information Text

Additional Materials and Methods

State assignments. We compared free energy values derived from our single-molecule records to predictions of secondary structure stability supplied by mfold (1). As in prior optical trapping work on RNA folding, free energy estimates were computed for 25 ºC (our experimental temperature) using mfold v2.3, with a salt correction scaling factor of 0.75 applied to the base-stacking energies (2, 3).

Although pseudoknot folds cannot be handled by mfold, the folding behavior of the P1 hairpin could be directly compared to predictions. Our experimental value, $\Delta G(0,\text{unfolded}\rightarrow\text{folded}) = \Delta G(0,\text{unfolded}\rightarrow\text{frayed}) + \Delta G(0,\text{frayed}\rightarrow\text{folded}) = -8.7 \pm 0.7$ kcal/mol, based on a kinetic analysis, closely matched the predicted value, $\Delta G_{\text{mfold}} = -8.5 \pm 0.4$ kcal/mol. Similarly, the unloaded P1 energetic stability derived from a thermodynamic analysis, -7.1 ± 0.8 kcal/mol, was also comparable to this prediction. The predicted stabilities of the unfolded-to-frayed and frayed-to-folded transitions also matched experimental results, within error. Comparisons of measured P1 folding energetics and mfold predictions are found in Table S2. The agreement of measured values and mfold predictions is similar to that observed in prior work on RNA hairpins (2, 3), and lends confidence to the accuracy of the optical force calibration, and to the assignment of these transitions to P1 unfolding via a frayed intermediate.

Folding dynamics between the fully unfolded and frayed P1 hairpin state were consistently observed in constant-force measurements, but full hairpin refolding from the frayed state was only observed in a subset of records. It seems likely that the frayed-to-folded transition is often obscured by noise and drift: this explanation would be consistent with a previous report by Woodside *et al.* (4) that the extension changes measured for a series of DNA hairpins corresponded to unfolding from an effective frayed state, comprised of an admixture of fully folded and partially unfolded states. Fraying behavior of the P1 hairpin is also consistent with the very "soft" unfolding transition seen in the corresponding force regime of FECs (Fig. 1C), suggestive of a multi-step unfolding process.

We also estimated the predicted basepairing free energy for P2.2 based on nearest-neighbor basepair energies and on the mfold-predicted free energy term for the single-base bulge found in this element. Because stacking interactions between P2.2 with P1 are not handled by mfold, and thus neither is the A8 bulge found by the last basepair of P2.2, we computed the sum of the predicted basepairing energy of bulge-free P2.2 (–8.7 kcal/mol) and the mfold energy increment corresponding to a single A-bulge followed by a G-C basepair (1.5 kcal/mol), yielding $\Delta G_{\mathrm{mfold}}$(P2.2 basepairing) = –7.1 ± 0.4 kcal/mol. This predicted value is considerably higher than the measured folding stability for P2.2: averaging over kinetic and thermodynamic results across all ligand conditions (Table S1), we obtained ΔG_{fold}(P2.2) ≈ –0.9 kcal/mol. The ~6 kcal/mol difference between the measured folding stability and the predicted free energy may reflect some combination of the entropic cost for loop-closure with the P2-P2.1 pseudoknot (which is required for P2.2 formation) and structural strain trapped in the P2.2 duplex fold (e.g. due to nonideal helix geometry).

The P2-P2.1 pseudoknot exhibited interesting properties. P2-P2.1 is only moderately stable ($\Delta G_{\mathrm{fold,P2\text{-}P2.1}}$ ~ –4 to –7 kcal/mol), and it unfolds at a lower force (10.0 pN) than a number of previously characterized RNA pseudoknots (5, 6) (Table S1). A reduced stability can be understood in light of its paucity of intra-pseudoknot tertiary contacts (just one: a base triple formed by A27 and the adjacent C28-G45 pair) (6), combined with an absence of stacking between the constituent P2.1 and P2 duplex elements (7, 8). We conclude that the P2-P2.1 pseudoknot element is essentially the sum of its secondary structure parts. However, the P2-P2.1 pseudoknot substructure normally exists in the context of the larger, P2-P2.1-P2.2 double pseudoknot. This double pseudoknot is stabilized mainly through tertiary contacts of P2.2 and P2.1 to the P1-P2.1 linker, and by tertiary stacking interactions (P2.2 stacks with P1 "above" and P2 "below" it, relative to the P2.2 first-strand 5′-3′ axis; Fig. 1A) (7, 8). Hence, while the ribozyme active site formed by the double pseudoknot is held together by a number of tertiary interactions, we find that its components (P2.2 duplex, P2-P2.1 pseudoknot) are not especially stable structures on their own.

Supplementary Figures and Tables

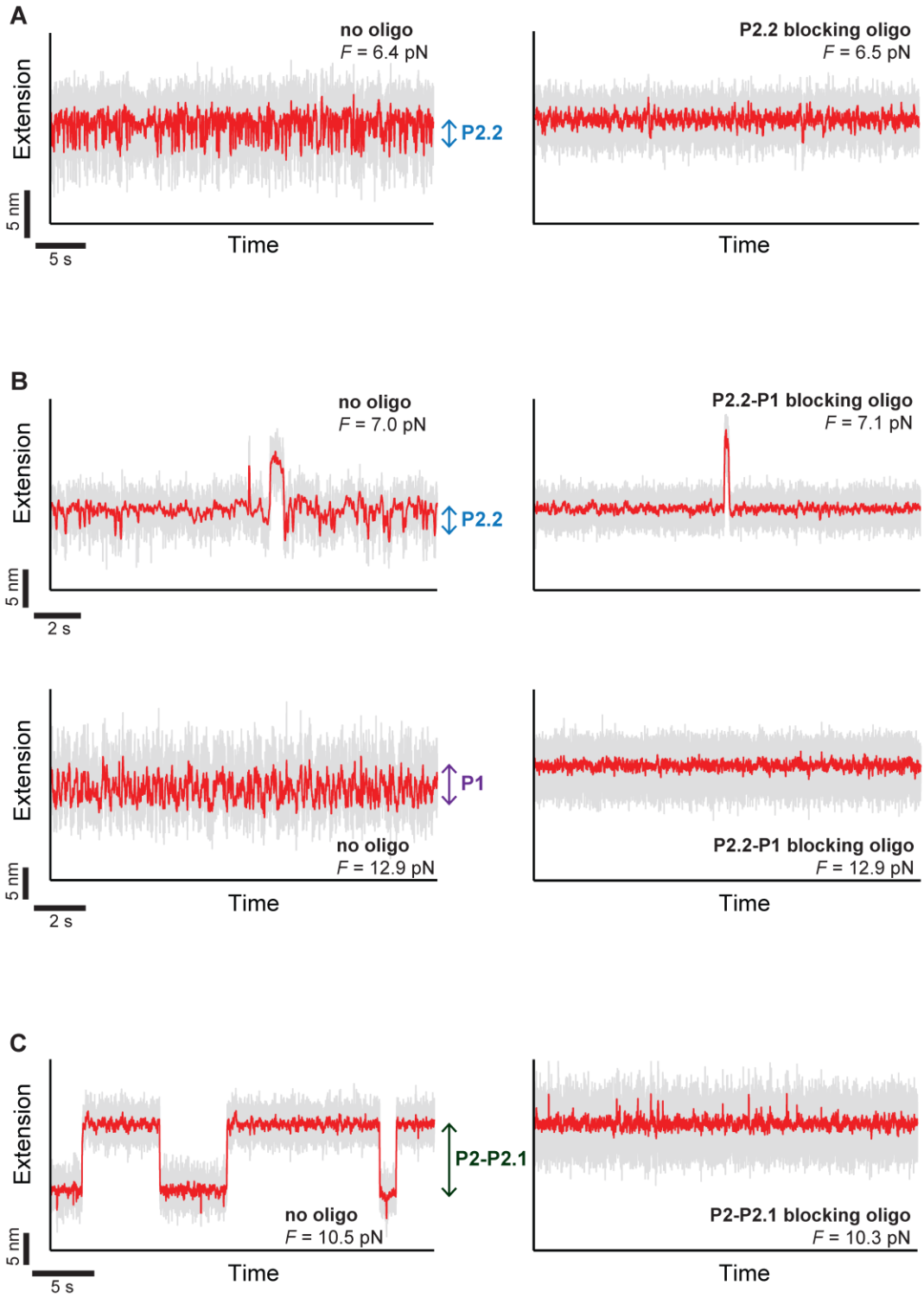

Fig. S1. Representative constant-force records from experiments with blocking oligonucleotides, supporting state assignments. Apo *glmS* ribozyme core folding dynamics are shown without (*left side*) and with (*right side*) the blocking oligo present.

(**A**) Blocking oligo (at 100 µM) complementary to the first strand of P2.2 (C2–G7, Fig. 1A) suppresses the transition assigned to P2.2 folding. (**B**) Blocking oligo (at 100 µM) complementary to the first strands of P2.2 and P1 (C2–A14, Fig. 1A) suppresses the transitions assigned to P2.2 folding (*top*) and P1 folding (*bottom*). (**C**) Blocking oligo (at 1 mM) for the P2-P2.1 pseudoknot, complementary to the first strand of P2 and the second strand of P2.1 (G34–A46, Fig. 1A), suppresses the transition assigned to P2-P2.1 pseudoknot folding and P1 hairpin reorientation (see Fig. 2C). Unsurprisingly, P2.2 folding (seen in the oligo-free trace as a transient fluctuation to lower extension from the P2-P2.1 folded state) is also blocked by the presence of P2-P2.1 pseudoknot blocking oligo.

Table S1. Summary of derived parameters and predicted extension changes, corrected for folded-state widths. For P2.2 folding, data are from N = 13 molecules for apo thermodynamics and N = 7 molecules for apo kinetics; N =23 molecules for +GlcN6P thermodynamics, N = 7 molecules for +Glc6P thermodynamics, and N = 5 molecules for +Glc6P kinetics. Data for P2-P2.1 folding are from N = 6 molecules. Data for two-step P1 folding (via a frayed state) are from N = 3 molecules.

	P2.2	**P2.2 +GlcN6P**	**P2.2 +Glc6P**	**P2-P2.1**	**P1 folded↔frayed**	**P1 frayed↔unfolded**
$F_{1/2}$, pN *	5.7 ± 0.3	5.2 ± 0.7	4.2 ± 0.7	10.0 ± 0.1	12.6 ± 0.2	14.2 ± 0.1
Δx, nm (Δx_{fit}, nm*)	2.2 ± 0.1 (1.8 ± 0.3)	1.7 ± 0.1 (2.2 ± 0.4)	2.3 ± 0.1 (2.1 ± 0.6)	8.7 ± 0.5 (7.4 ± 0.8)	2.6 ± 0.1 (2.7 ± 0.4)	2.9 ± 0.3 (3.7 ± 0.3)
Δx_{pred}, nm†	2.5 ± 0.3	2.4 ± 0.2	2.1 ± 0.2	12.3 ± 1.2	2.5 ± 0.2	2.8 ± 0.3
$\Delta x^{\ddagger}_{fold}$, nm	1.7 ± 0.4	—	1.8 ± 0.3	4.4 ± 0.7	1.2 ± 0.2	2.4 ± 0.2
$\Delta x^{\ddagger}_{unf}$, nm	0.8 ± 0.1	—	0.7 ± 0.2	2.0 ± 0.6	1.5 ± 0.1	1.20 ± 0.04
$\tau_{unfolded}(0)$, ms	4.6 ± 2.8	—	5.1 ± 2.5	(5.4 ± 9.1) × 10^{-2}	(7.9 ± 5.3) × 10^{-1}	(8.2 ± 7.9) × 10^{-3}
$\tau_{folded}(0)$, ms	140 ± 30	—	64 ± 17	(3.9 ± 5.6) × 10^{5}	(3.1 ± 1.0) × 10^{3}	(2.8 ± 0.5) × 10^{3}
$k_{fold}(0)$, s^{-1}	220 ± 130	—	200 ± 100	(1.8 ± 3.1) × 10^{4}	(1.3 ± 0.9) ×·10^{3}	(1.2 ± 1.2) × 10^{5}
$k_{unfold}(0)$, s^{-1}	7.1 ± 1.7	—	16 ± 4	(2.6 ± 3.7) × 10^{-3}	(3.2 ± 1.1) ×·10^{-1}	(3.6 ± 0.6) ×·10^{-1}
$k_{1/2}$, s^{-1}	21 ± 5	—	33 ± 9	0.33 ± 0.48	33 ± 17	25 ± 17
$F_{1/2}$, pN (kinetic)	5.6 ± 0.3	—	4.0 ± 0.3	10.2 ± 0.2	12.7 ± 0.1	14.4 ± 0.1
$\Delta G_{fold}(0)$, kcal/mol (thermodynamic)	–1.0 ± 0.1	–0.9 ± 0.4	–0.6 ± 0.2	–6.9 ± 0.7	–3.6 ± 0.6	–3.5 ± 0.6
$\Delta G_{fold}(0)$, kcal/mol (kinetic)	–1.2 ± 0.4	—	–0.7 ± 0.3	–3.6 ± 1.3	–3.7 ± 0.4	–5.0 ± 0.6
$\Delta G^{\ddagger}_{fold}(0)$, kcal/mol	3.6 ± 0.4	—	3.7 ± 0.3	1.0 ± 1.0	2.6 ± 0.4	–0.1 ± 0.6
$\Delta G^{\ddagger}_{unf}(0)$, kcal/mol	5.6 ± 0.1	—	5.2 ± 0.2	10.3 ± 0.9	7.5 ± 0.2	7.4 ± 0.1

*: parameters from Boltzmann fit to $P_{folded}(F)$

†: assumes ±10% uncertainty for WLC predicted Δx

Table S2. Folding stabilities for two-step P1 folding compared with mfold predictions.

	P1 folded↔frayed	**P1 frayed↔unfolded**	**P1 folded↔unfolded**
$\Delta G_{fold}(0)$, kcal/mol (thermodynamic)	–3.6 ± 0.6	–3.5 ± 0.6	–7.1 ± 0.8 (*)
$\Delta G_{fold}(0)$, kcal/mol (kinetic)	–3.7 ± 0.4	–5.0 ± 0.6	–8.7 ± 0.7 (*)
$\Delta G_{fold}(0)$, kcal/mol (mfold prediction)	–4.1 ± 0.4 (†)	–4.4 ± 0.2	–8.5 ± 0.4

*: Sum of measured values from unfolded-to-frayed and frayed-to-folded steps
†: based on ΔG_{mfold}(frayed→folded) = ΔG_{mfold}(unfolded→folded) – ΔG_{mfold}(unfolded→frayed)

Table S3. Parameters from fit to force-dependence of the +GlcN6P self-cleavage rate.

$F_{max/2}$, pN	k_{max}, min^{-1}	k_{min}, min^{-1}	Δx, nm
4.8 ± 1.2	1.7 ± 0.8	0.09 ± 0.33	3.4 ± 4.1

Table S4. Comparison of average unloaded lifetimes for P2.2 folded and unfolded states (average of apo and +Glc6P results; Table S1) compared to the unloaded self-cleavage survival time, determined from fit of $k_{obs(clvg)}$ vs. F.

P2.2 $\tau_{unfolded}(0)$, ms	**P2.2 $\tau_{folded}(0)$, ms**	**Survival time, $1/k_{obs(clvg)(0)}$, ms**
4.8 ± 1.9	100 ± 20	$(3.6 \pm 2.0) \times 10^4$

References:

1. Zuker M (2003) Mfold web server for nucleic acid folding and hybridization prediction. *Nucleic Acids Research* 31(13):3406-3415.

2. Greenleaf WJ, Frieda KL, Foster DAN, Woodside MT, & Block SM (2008) Direct observation of hierarchical folding in single riboswitch aptamers. *Science* 319(5863):630-633.

3. Liphardt J, Onoa B, Smith SB, Tinoco I, & Bustamante C (2001) Reversible unfolding of single RNA molecules by mechanical force. *Science* 292(5517):733-737.

4. Woodside MT, *et al.* (2006) Direct measurement of the full, sequence-dependent folding landscape of a nucleic acid. *Science* 314(5801):1001-1004.

5. Ritchie DB, Foster DAN, & Woodside MT (2012) Programmed-1 frameshifting efficiency correlates with RNA pseudoknot conformational plasticity, not resistance to mechanical unfolding. *Proc Natl Acad Sci USA* 109(40):16167-16172.

6. Chen G, Chang KY, Chou MY, Bustamante C, & Tinoco I, Jr. (2009) Triplex structures in an RNA pseudoknot enhance mechanical stability and increase efficiency of -1 ribosomal frameshifting. *Proc Natl Acad Sci USA* 106(31):12706-12711.

7. Cochrane JC, Lipchock SV, & Strobel SA (2007) Structural investigation of the GlmS ribozyme bound to Its catalytic cofactor. *Chem Biol* 14(1):97-105.

8. Klein DJ & Ferre-D'Amare AR (2006) Structural basis of glmS ribozyme activation by glucosamine-6-phosphate. *Science* 313(5794):1752-1756.